Available online at www.sciencedirect.com
ScienceDirect
Solid State Ionics 178 (2007) 253–257
SOLID STATE IONICS
www.elsevier.com/locate/ssi

In situ synchrotron diffraction study of high temperature prepared orthorhombic $LiMnO_2$

Y.J. Wei [a], H. Ehrenberg [b,d,*], N.N. Bramnik [b], K. Nikolowski [b], C. Baehtz [c], H. Fuess [b]

[a] College of Materials Science and Engineering, Jilin University, Changchun, 130023, China
[b] Darmstadt University of Technology, Institute for Materials Science, Petersenstr. 23, D-64287 Darmstadt, Germany
[c] Deutsches Elektronensynchrotron (DESY), Notkestr. 85, D-22607 Hamburg, Germany
[d] Institute for Complex Materials, Leibniz Institute for Solid State and Materials Research, Helmholtzstr. 20, D-01069 Dresden, Germany

Received 28 July 2006; received in revised form 16 October 2006; accepted 30 November 2006

Abstract

$HT\text{-}LiMnO_2$ was prepared by a solid-state reaction at 900 °C. Electrochemical charge–discharge cycling of $HT\text{-}LiMnO_2$ showed an initial charge capacity 113 mA h g^{-1}, followed by a small first discharge of 25 mA h g^{-1}. The discharge capacity subsequently increased and reached up to ~120 mA h g^{-1} after 30 cycles. In situ synchrotron diffraction showed that $HT\text{-}LiMnO_2$ transformed to a new phase (Phase II) during the first charge process, which was metastable and could easily convert to spinel $LiMn_2O_4$ in the following cycles. The progressive formation of this spinel phase was responsible for the capacity increase of the battery in the first cycles. The different cycling performance of $HT\text{-}LiMnO_2$ and $LT\text{-}LiMnO_2$ was attributed to the large stacking faults in $LT\text{-}LiMnO_2$, which may facilitate the material to completely convert to spinel $LiMn_2O_4$ in the first charge without the medium transition to Phase II.

Keywords: Orthorhombic $LiMnO_2$; Lithium ion battery; Structural properties; In situ diffraction; Electrochemical properties

1. Introduction

The cathode material $LiCoO_2$ has been intensively used in marketable lithium ion batteries since its first introduction into market in the 1990s. Despite the success of $LiCoO_2$, the development of a future generation of lithium batteries is critically dependent on replacing this cathode material. In recent years, extensive attention has been devoted to Li–Mn–O compounds due to their higher capacities and voltages, lower cost and toxicity than $LiCoO_2$. Lithium batteries using spinel $LiMn_2O_4$ as cathode materials have been intensively studied and are already in the process of commercialization [1–3]. However, $LiMn_2O_4$ still faces some problems such as the gradual capacity fading upon cycling especially at high temperatures above 50 °C, as well as its limited reversible capacity ~120 mA h g^{-1}. Li–Mn–O compounds with the formula of $LiMnO_2$ would be an ideal choice, provided most of the lithium could be extracted–inserted since this corresponds to a much higher capacity of 285 mA h g^{-1} than $LiMn_2O_4$.

Depending on synthetic conditions, $LiMnO_2$ can form either a monoclinic structure with space group $C/2m$, or an orthorhombic structure with space group Pmnm. The former one has been successfully prepared by a lithium/sodium exchange reaction from α-$NaMnO_2$ [4–6]. It has been well demonstrated that the so-prepared compound is metastable, which will completely transform to a spinel $LiMn_2O_4$ phase within a few charge–discharge cycles [7]. Recently, numerous attention has been devoted to orthorhombic $LiMnO_2$ aiming at the marketable use of this material. Different research groups have prepared orthorhombic $LiMnO_2$ at low temperatures (T<450 °C, herein marked by $LT\text{-}LiMnO_2$) [8,9] or high temperatures (T>800 °C, herein marked by $HT\text{-}LiMnO_2$) [10,11]. It was shown that the structure of $LT\text{-}LiMnO_2$ could be described by introducing an amount of stacking faults into the ideal structure of $HT\text{-}LiMnO_2$. Kötschau and Dahn reported by means of in situ X-ray diffraction (XRD) that $LT\text{-}LiMnO_2$

* Corresponding author. College of Materials Science and Engineering, Jilin University, Changchun, 130023, China; Darmstadt University of Technology, Institute for Materials Science, Petersenstr. 23, D-64287 Darmstadt, Germany. Tel.: +49 6151 164391; fax: +49 6151 166023.
E-mail address: ehrenberg@tu-darmstadt.de (H. Ehrenberg).

0167-2738/$ - see front matter © 2007 Elsevier B.V. All rights reserved.
doi:10.1016/j.ssi.2006.11.018

converts irreversibly to a spinel $LiMn_2O_4$ phase after the first charge [12]. The subsequent first discharge delivered a high Li^+ capacity near 200 mA h g^{-1}, which could maintain a good reversibility over long term cycling.

It has often been stated in the past that HT-$LiMnO_2$ phases were not good cathode materials for lithium batteries [9,13]. However, numerous recent works on HT-$LiMnO_2$ have shown promising battery use of these materials provided they were properly prepared. The electrochemical cycling of these HT-$LiMnO_2$ were characterized by a small discharge capacity about several tens mA h g^{-1} in the first cycle, which then subsequently increased to 120–160 mA h g^{-1} in the following 10–30 cycles. The materials afterwards exhibited good cycling performance over hundreds of cycles. Croguennec et al. pointed out that a large surface area and a high Li/Mn cationic exchange ratio are necessary factors for the good electrochemical performance of HT-$LiMnO_2$ [14].

Former ex situ XRD studies have shown that the structure transition to spinel $LiMn_2O_4$ is also unavoidable for HT-$LiMnO_2$ [15,16]. After a careful comparison one may see that the cycling behavior of HT-$LiMnO_2$ is somewhat different from that of LT-$LiMnO_2$. The latter shows almost no gradual capacity increase in the initial cycles as occurring for HT-$LiMnO_2$, but directly reaches the reversible capacity (~200 mA h g^{-1}) already after the first cycle [12,17]. Accordingly, different structural transitions in the initial electrochemical cycles are expected for HT- and LT-$LiMnO_2$. The details of the structural transition of HT-$LiMnO_2$ can be revealed by in situ synchrotron diffraction using high-energy radiation. In this work, we employed in situ synchrotron diffraction to study the structural properties of HT-$LiMnO_2$ in order to elucidate the difference in the structural changes of HT-$LiMnO_2$ and LT-$LiMnO_2$ during electrochemical process.

2. Experimental

HT-$LiMnO_2$ was prepared by a solid-state reaction method. The precursor was a mixture of $LiNO_3$ (Aldrich company, 99.99%) and $Mn(NO_3)_2{\cdot}4H_2O$ (Merck company, 98%) weighted in a Li:Mn molar ratio of 1.02. A small excess of lithium was added to compensate for lithium evaporation at high temperatures. The homogeneous mixture was initially heat treated at 400 °C for 5 h. Then the resultant powder was pressed into a pellet and heated at 500 °C for 3 h in Ar atmosphere to ensure the complete decomposition of the starting materials. The furnace temperature was subsequently raised up to 900 °C at a speed of 1 °C min^{-1}. The pellet was then sintered at this temperature for 12 h to obtain the target material.

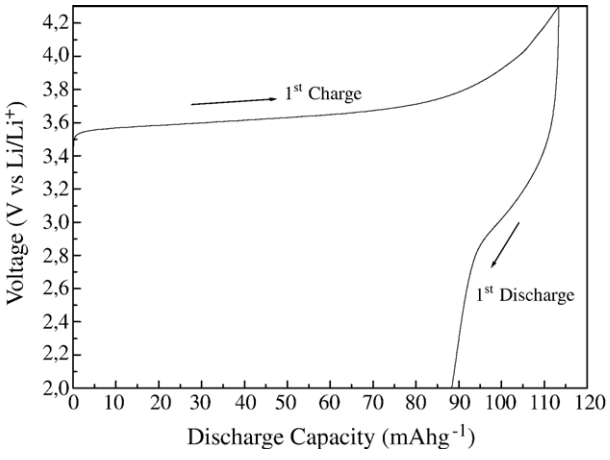

Fig. 1. The first charge–discharge potential profiles of the Li|HT-$LiMnO_2$ cell.

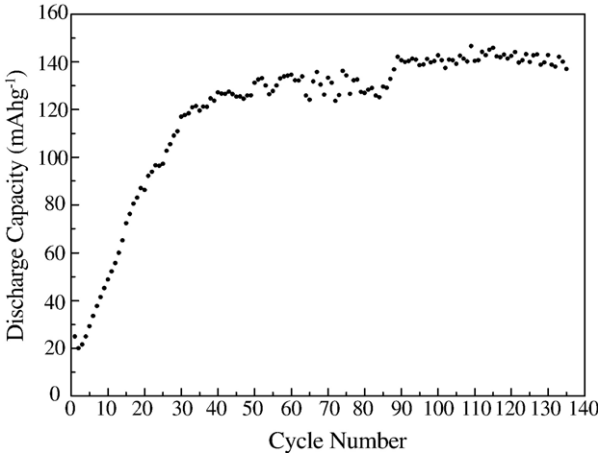

Fig. 2. The discharge capacities versus cycle numbers of the Li|HT-$LiMnO_2$ cell cycled in the potential region 4.3–2.0 V with the current density 40 mA g^{-1}.

Electrochemical charge–discharge cycling was carried out with a multichannel potentiostatic–galvanostatic electrochemical interface VMP (Perkin Elmer Instruments, USA). A Swagelok-type cell was assembled in an argon-filled glove box with H_2O and O_2 contents less than 1 ppm. For the fabrication of the cathode electrode, 80% active material, 15% acetylene carbon black and 5% poly-vinylidenefluoride were intimately mixed, and then pressed onto an Al-mesh. The resulting electrode contained 8.85 mg of active material. The electrolyte was a 1 M solution of $LiPF_6$ in EC:DMC (2:1 by volume ratio) soaked in a glass–fiber separator. The current density for the charge–discharge cycling was 40 mA g^{-1} (~C/7).

In situ synchrotron diffraction was carried out in transmission mode at the powder diffraction beamline B2 of the Deutsches Elektronensynchrotron (DESY) at Hamburg, Germany. The battery was a modified Swagelok-type cell [18]. It consists of a lithium anode, separator soaked with electrolyte and a cathode electrode which is a pellet containing 17 mg of active material. The aluminum cathode holder and copper anode holder served as current collectors. The cell was mounted on a flat sample holder, which can be oscillated to reduce preferred orientation effects and enhance powder statistics. A wavelength of λ=0.47189 Å was selected by a double-crystal Si (111) monochromator. The current density was 10 mA g^{-1} (~C/28) during the collection of in situ diffraction data. The diffraction data of the 1, 13 and 28th cycle were recorded using the on-site readable image-plate detector OBI [19]. The intermediate cycles were performed off side the beam to enable measurements on more different samples and with a higher current density of 40 mA g^{-1} to reach higher cycle numbers within the fixed

period of allocated beam time. Rietveld refinement was applied for data analysis using the WinplotR package [20].

3. Results and discussion

Galvanostatic cycling was carried out for the Li|HT-$LiMnO_2$ cell in the potential region 4.3–2.0 V. Fig. 1 displays the charge–discharge potential profiles of the first cycle. The charge–discharge cycling of this battery started with the removal of Li^+ from $LiMnO_2$, which gained a charge capacity 113 mA h g^{-1}. The following first discharge delivered a much lower capacity of 25 mA h g^{-1}. The first charge potential profile was dominated by a voltage plateau around 3.6 V, which was absolutely different from that of the subsequent first discharge. This indicates an irreversible structural change taking place in the cathode material during the first charge process. Fig. 2 displays the discharge capacities versus cycle numbers of the battery cell. The discharge capacity subsequently increased and reached up to ~120 mA h g^{-1} after 30 cycles. The material thus exhibited a good cycle life, showing a reversible discharge capacity 120–140 mA h g^{-1} over 130 cycles.

Fig. 3(a) shows the synchrotron diffraction pattern of the fresh battery cell. Rietveld refinement of the pristine HT-$LiMnO_2$ was performed using the structural model in Ref. [21]. It was confirmed that the pristine cathode material was orthorhombic $LiMnO_2$, crystallizing in the space group P*mnm*. Additional diffraction peaks could be attributed to the Li anode and Al current collector. The structural parameters listed in Table 1 show that the present HT-$LiMnO_2$ had a large cationic disorder on the lithium and manganese sites, *i.e.* about 14% of the Li positions are occupied by Mn and vice versa. This large cationic disorder in HT-$LiMnO_2$ is reasonable considering that the Li^+ and Mn^{3+} cations have similar size in octahedral environment (Li^+: 0.76 Å, Mn^{3+}: 0.645 Å) [22], and both of them occupy the (2a) sites. Croguennec et al. pointed out that the presence of Mn within the Li sheets may improve the electrochemical behavior of the disordered materials compared with that of the ordered phase [16].

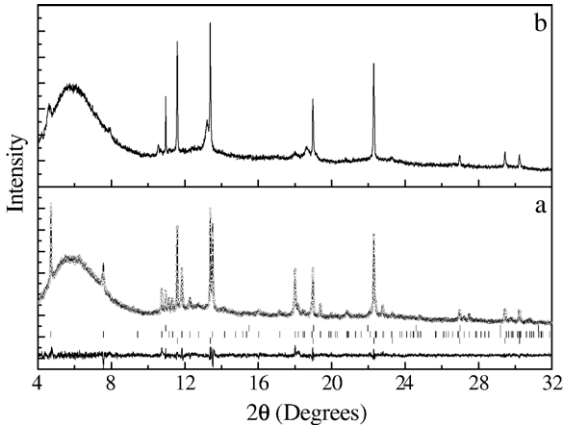

Fig. 3. The synchrotron diffraction patterns of (a) the fresh battery cell, and (b) at the end of the first charge. The Rietveld refinement results of the pattern (a) are attached. The reflection marks belong to the phases of Li, HT-$LiMnO_2$ and Al from top to bottom. The Bragg *R* value for HT-$LiMnO_2$ is 10.8%.

Table 1
The Rietveld refined structural parameters of HT-$LiMnO_2$

Phase	Atom*	Atom position			Site occupancy (%)
		x	*y*	*z*	
HT-$LiMnO_2$**	Li (1)	0.25000	0.08838	0.25000	0.21436 (86%)
	Li (2)	0.25000	0.62050	0.25000	0.03564 (14%)
	Mn (1)	0.25000	0.08838	0.25000	0.03564 (14%)
	Mn (2)	0.25000	0.62050	0.25000	0.21436 (86%)
	O (1)	0.75000	0.14357	0.25000	0.25000 (100%)
	O (2)	0.75000	0.62629	0.25000	0.25000 (100%)

*The isotropic displacement parameters were fixed at 0.5 $Å^2$ for Mn and 1.0 $Å^2$ for Li and O.
**Cell parameters: a=4.5725 (1) Å; b=5.7419 (2) Å; c=2.8037 (1) Å; $\alpha=\beta=\gamma=90°$.

Fig. 3(b) displays the in situ diffraction pattern of HT-$LiMnO_2$ collected at the end of the first charge (state of charge: 4.3 V). Note that this in situ cell gained a larger first charge capacity 130 mA h g^{-1} than the above Swagelok cell due to the much lower current density employed. Two selected 2θ regions of the total 32 in situ diffraction patterns, $4.2°<2\theta<5.1°$ and $17°<2\theta<20°$, are displayed in Fig. 4 to show the structural evolution of HT-$LiMnO_2$ during the first charge. It is seen from Fig. 4 that the intensities of the (010), (221), (131) and (002) peaks of orthorhombic $LiMnO_2$ decreased with Li^+ extraction. In the mean while, two new peaks appeared at $2\theta=4.55$ and 18.5°, and their intensities progressively increased. Based on these observations it can be stated that orthorhombic $LiMnO_2$ transformed into a new phase (marked by Phase II) during the first charge process, which was consistent with the voltage plateau at ~3.6 V on the first charge potential profile (Fig. 2). It

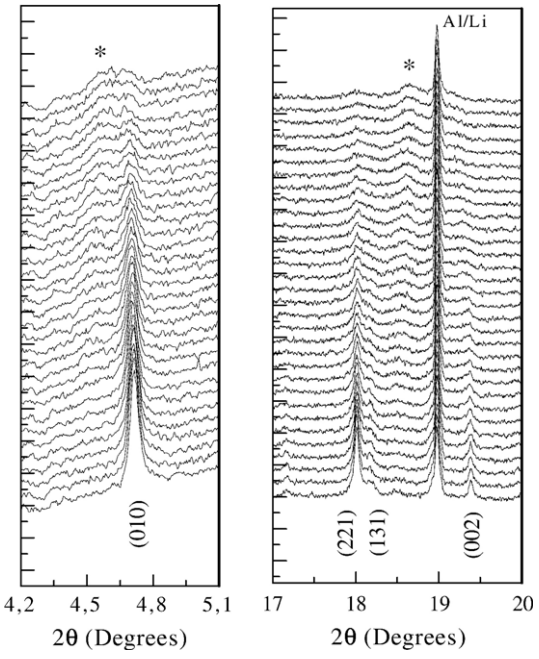

Fig. 4. The selected 2θ regions of the total 32 in situ diffraction patterns of HT-$LiMnO_2$ during the first charge. The diffraction peaks marked by "*" are assigned to Phase II.

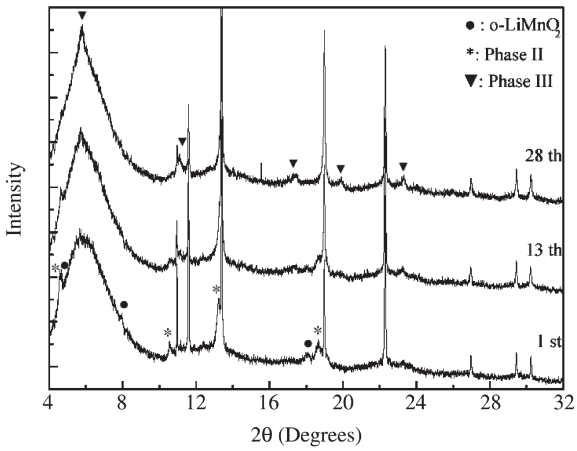

Fig. 5. The diffraction patterns of the cathode material after 1, 13 and 28 cycles, collected at the state of charge 4.3 V.

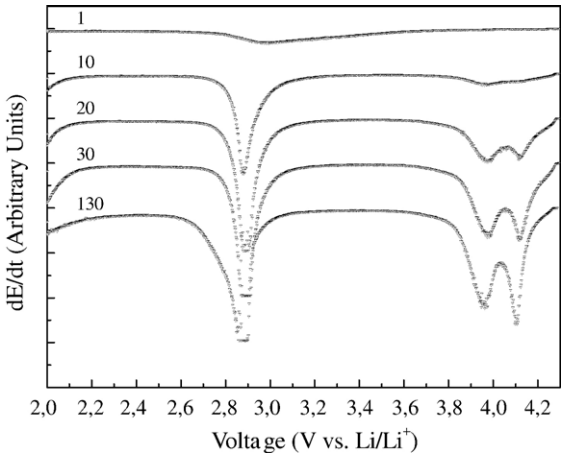

Fig. 7. The incremental capacities versus discharge potentials of the Li|HT-$LiMnO_2$ cell.

is observed that both the diffraction peaks of HT-$LiMnO_2$ and those of the newly formed phase became broader and broader with Li^+ extraction. This suggests the formation of defects (*e.g.* microstrain and stacking faults) in the material lattice, or that the crystal particles cracked into some smaller ones during the electrochemical process. On the other hand, even though the peak intensities of the HT-$LiMnO_2$ phase decreased with Li^+ extraction, they didn't disappear completely after the first charge. This indicates that a proportion of HT-$LiMnO_2$ didn't participate in the initial electrochemical process and remained in the cathode electrode.

It is mandatory to clarify the crystal structure of Phase II since it is closely related to the electrochemical properties of HT-$LiMnO_2$. However, up to now there is not a definite description on the crystal structure of this new phase. Croguennec et al. have suggested that it might have a spinel or hexagonal structure [14]. But there are no experimental facts to support this proposal. It has been well documented that the first diffraction peak of Li–Mn–O spinel or hexagonal structures is located at d spacing ≈4.7 Å [16,23]. However, the present in situ diffraction patterns in Fig. 4 clearly show that the first diffraction peak of Phase II appeared at $d \approx 5.9$ Å ($2\theta \approx 4.56°$). This is rather a big value that cannot be assigned to either a spinel or a hexagonal structure. We have tried to refine Phase II using spinel, hexagonal and other structural models. But none of them gave a satisfactory result. At present we will not concentrate on this challenge but continue to investigate how Phase II behaves during the following cycles.

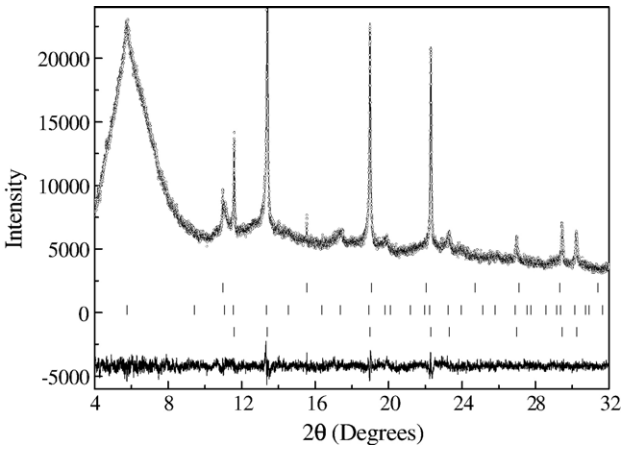

Fig. 6. The Rietveld refinement of the synchrotron diffraction pattern collected after 28 cycles. The reflection marks belong to the phases of Li, Phase III and Al from top to bottom. The Bragg R value for Phase III is 7.65%.

Fig. 5 displays the diffraction patterns of the cathode material after 1, 13 and 28 cycles, collected at the state of charge 4.3 V. The intensities of the diffraction peaks belonging to Phase II and non-reacted HT-$LiMnO_2$ decreased with cycling. Meanwhile, some new peaks appeared at $2\theta \approx 5.77$, 11.06, 17.36, 19.79 and 23.22°, which are characteristics of the formation of a new phase (marked by Phase III). Both Phase II and the non-reacted HT-$LiMnO_2$ could not be observed from the diffraction pattern after 28 cycles, indicating that the cathode material completely transformed to Phase III. Rietveld refinement was carried out on Phase III (Fig. 6) and confirmed it has a typical spinel structure with the cell parameter $a = 8.1239$ Å.

The incremental capacities versus discharge potentials of the Li|HT-$LiMnO_2$ cell are plotted in Fig. 7 in order to determine the electrochemical redox potentials of the cathode material. It is seen from the figure that three incremental peaks appeared at ~2.88, 3.96 and 4.11 V, and their intensities increased with cycling. The enhancement of the incremental peaks was proportional to the amount of active cathode material participating in the Li^+ insertion process. It is noticed that the peak positions are very similar to those obtained from spinel $LiMn_2O_4$: the one located at 2.88 V corresponds to Li^+ insertion into the octahedral sites, while the other two at 3.96 and 4.11 V are due to Li^+ insertion into the tetrahedral sites. These observations suggest that the spinel phase (Phase III) progressively formed in the initial charge–discharge cycles was the active material providing the discharge capacities of the Li|HT-$LiMnO_2$ battery. Note that a trace of Phase III could be observed on the diffraction pattern after the first charge (Fig. 5), which caused the small first discharge capacity 25 mA h g^{-1} of the material.

4. Conclusions

We have pointed out that HT-$LiMnO_2$ and LT-$LiMnO_2$ may undergo different structural transitions in the initial electrochemical stage since they exhibit different cycling performance. According to Dahn's work, LT-$LiMnO_2$ completely converts to a spinel $LiMn_2O_4$ phase after the first charge. The present study showed different structural properties for HT-$LiMnO_2$, which underwent an irreversible structural transition from orthorhombic to a new phase (Phase II) during the first charge. Up to now the crystal structure of Phase II was not resolved. However, it can be stated that Phase II only acts as a transition phase during the electrochemical process. It is metastable and can easily transform to a spinel $LiMn_2O_4$ phase in the following cycles. This spinel phase is the active material that contributes to the discharge capacities of the battery.

The small first discharge capacity of HT-$LiMnO_2$ was attributed to the slight spinel phase that formed during the first charge. Therefore, it is obvious that the structural conversion from orthorhombic to spinel is much easier for LT-$LiMnO_2$ than for HT-$LiMnO_2$, because LT-$LiMnO_2$ completely converts to spinel $LiMn_2O_4$ already after the first charge. Considering the difference in microstructures of LT- and HT-$LiMnO_2$, it can be suggested that the different structural properties of the two $LiMnO_2$ phases are attributed to the large stacking faults in LT-$LiMnO_2$, which may facilitate the material to completely convert to the spinel phase in the first charge without the medium transition to Phase II.

Acknowledgement

This work was financially supported by the Deutsche Forschungsgemeinschaft (DFG) in the frame of project Sonderforschungsbereich 595 "Electrical fatigue in functional materials" and by the special funds for major state basic research project (973) of China under the Grant 2002CB211802.

References

[1] H. Gadjov, M. Gorova, V. Kotzeva, G. Avdeev, S. Uzunova, D. Kovacheva, J. Power Sources 134 (2004) 110.
[2] Y.J. Wei, K.W. Nam, K.B. Kim, G. Chen, Solid State Ionics 177 (2006) 29.
[3] M.R. Palacín, Y. Chabre, L. Dupont, M. Hervieu, P. Strobel, G. Rousse, C. Masquelier, M. Anne, G.G. Amatucci, J.M. Tarascon, J. Electrochem. Soc. 147 (2000) 845.
[4] A.R. Armstrong, P.G. Bruce, Nature 381 (1996) 499.
[5] Y. Shao-Horn, S.A. Hackney, A.R. Armstrong, P.G. Bruce, R. Gitzendanner, C.S. Johnson, M.M. Thackeray, J. Electrochem. Soc. 146 (1999) 2404.
[6] F. Capitaine, P. Gravereaub, C. Delmas, Solid State Ionics 89 (1996) 197.
[7] G. Vitins, K. West, J. Electrochem. Soc. 144 (1997) 2587.
[8] T. Ohzuku, A. Ueda, T. Hirai, Chem. Express 7 (1992) 193.
[9] J.N. Reimers, Erick W. Fuller, Erick Rossen, J.R. Dahn, J. Electrochem. Soc. 140 (1993) 3396.
[10] Y.S. Lee, Y.K. Sun, K. Adachi, M. Yoshio, Electrochim. Acta 48 (2003) 1031.
[11] Y. Idemoto, T. Mochizuki, K. Ui, N. Koura, J. Electrochem. Soc. 153 (2006) A418.
[12] I.M. Kötschau, J.R. Dahn, J. Electrochem. Soc. 145 (1998) 2672.
[13] R.J. Gummow, D.C. Liles, M.M. Thackeray, Mater. Res. Bul. 28 (1993) 1249.
[14] L. Croguennec, P. Deniard, R. Brec, P. Biensan, M. Broussely, Solid State Ionics 89 (1996) 127.
[15] Jung-Min Kim, Hoon-Taek Chung, J. Power Sources 115 (2003) 125.
[16] L. Croguennec, P. Deniard, R. Brec, J. Electrochem. Soc. 144 (1997) 3323.
[17] I. Kötschau, M.N. Richard, J.R. Dahn, J.B. Soupart, J.C. Rousche, J. Electrochem. Soc. 142 (1995) 2906.
[18] K. Nikolowski, C. Baehtz, N.N. Bramnik, H. Ehrenberg, J. Appl. Crystallogr. 38 (2005) 851.
[19] M. Knapp, V. Joco, C. Baehtz, H.H. Brecht, A. Berghaeuser, H. Ehrenberg, H. von Seggern, H. Fuess, Nucl. Instrum. Methods A521 (2004) 565.
[20] T. Roisnel, J. Rodriguez-Carvajal, Mater. Sci. Forum 118 (2001) 378.
[21] L. Croguennec, P. Deniard, R. Brec, A. Lecerf, J. Mater. Chem. 5 (1995) 1919.
[22] R.D. Shannon, Acta Crystallogr. A 32 (1976) 751.
[23] Inorganic Crystal Structure Database, Forschungszentrum Karlsruhe, Germany, Version 2006–01.